

Ion traps with enhanced optical and physical access

Robert Maiwald* and Gerd Leuchs

*Institute of Optics, Information and Photonics, Max Planck Research Group,
University Erlangen-Nuremberg, 91058 Erlangen, Germany*

Dietrich Leibfried,[†] Joe Britton, J. C. Bergquist, and D. J. Wineland
National Institute of Standards and Technology, Boulder, CO 80305, USA

(Dated: 15th October 2008)

We experimentally characterized a novel radio-frequency (rf) ion trap geometry formed by two concentric cylinders over a ground plane. These traps allow optical and physical access of 91 % and 96 % of 4π , respectively, in two of the three traps tested. We discuss fabrication of the traps, their characterization by use of single laser cooled $^{24}\text{Mg}^+$ ions and some potential applications of similar trap structures in quantum optics, electric and magnetic field sensing and microscopy.

PACS numbers: 37.10.Ty, 42.50.Ct

I. INTRODUCTION

Small, controllable and highly accessible quantum systems that are well isolated from their environment can serve as a probe at the single quantum level to study a multitude of effects, including fundamental processes of nature. Some prominent realizations of isolated quantum systems are quantum dots, Josephson junctions and trapped neutral atoms and atomic ions. The last two examples have been particularly successful and valuable tools to the field of quantum optics. In this paper we discuss a special trap geometry for confining atomic ions that provides largely unrestricted optical access. We theoretically modeled and experimentally demonstrated three traps with different levels of optical and physical access to the ion and characterized the trade-offs between ion confinement properties and access. Based on our findings we also discuss several possible applications that might take advantage of this open geometry.

In section II we introduce the basic trap geometry and theoretically model the trapping fields. Section III describes the construction of three different traps derived from the geometry with different levels of optical and physical access. Experimental characterization of the traps with the use of single laser-cooled $^{24}\text{Mg}^+$ ions is described in section IV. Possible applications of such traps in quantum optics and dynamical surface characterization and microscopy are briefly discussed in sections V and VI.

II. BASIC TRAP GEOMETRY

The primary design goal of the traps described here is to maximize the accessible solid angle to the ion for optical excitation and fluorescence collection while maintain-

ing good trapping properties. In addition to enhanced optical access to the ion, the geometry also allows for bringing surfaces close to a single ion that can be used as a sensitive probe for electromagnetic fields. Previous approaches for ion traps with enhanced optical access included traps consisting of two opposed sets of electrodes (endcap traps) [1, 2]. The design presented here provides easier indexing and assembly of the trap electrodes, with access to a large fraction of the 4π solid angle surrounding the ion.

The trap design consists of a cylindrical ground electrode coaxial with a larger diameter cylindrical radio-frequency (rf) electrode (see Fig. 1b). Similar planar trap geometries have been investigated for Penning traps [3, 4] and rf-trap arrays [5], but the traps discussed here allow for increased optical access by not having the electrodes lie in a common plane. To achieve a confining rotationally symmetric quadrupole potential, a grounded plane was placed at the base of the two cylindrical electrodes. Four additional electrodes were placed on a circle between the grounded plane and the rf electrode (see inset in Fig. 1b). By applying independent potentials to the four electrodes we can superimpose a static quadrupole field over the rf trapping potential to break its rotational symmetry. This enables laser Doppler cooling of all three normal modes of the trap with one laser beam. By individually biasing the four electrodes we can also compensate electric stray fields to minimize micromotion in the trap [6].

Simulations of the resulting pseudopotential generated by the electrode configuration described above indicate smaller trap potential depths and binding frequencies compared to those of more traditional trap designs of similar size, rf-drive frequency and amplitude (see Fig. 1a). Three different traps were built adjacent to each other onto the same test set-up. These traps range from a more conservative design with larger trap depth and motional frequencies and a smaller accessible solid angle to a weaker trap with greater optical access. This change in properties is achieved by varying the protrusion height Δ of the central grounded electrode with respect to the rf

*Electronic address: Robert.Maiwald@physik.uni-erlangen.de

[†]Electronic address: dil@boulder.nist.gov

electrode (see Fig. 1b) and results in the three electrode configurations #1, #2 and #3 as detailed in Table I.

III. TRAP CONSTRUCTION

The trap electrodes are made of stainless steel hypodermic tubing and hardened stainless steel rods. Structural integrity and insulation is provided by a combination of cylindrical alumina spacers and different layers of laser-cut alumina and micro-machined Macor (see Fig. 1c). We chose this approach to trap construction rather than following the newer developments in micro-fabricated traps [5, 8, 9, 10] because our design required aspect ratios of the electrodes that are difficult to achieve with microfabrication. Electrical connections were made by resistive welding of gold ribbons to the different steel electrodes and to gold traces that were silk-screened onto the alumina plates with a thickness of ~ 5 to $10 \mu\text{m}$. The ground plane at the base of the cylindrical electrodes is formed by a silk-screened gold layer applied to one side of the top alumina plate. All insulating surfaces have been recessed or placed to prevent a direct line of sight to the ion position. This suppresses distortions of the trapping field caused by charged insulating surfaces. The control potentials to the DC electrodes (central ground and compensation electrodes $A - D$, see inset of Fig. 1b) are passively filtered by RC low-pass filters with $R = 1 \text{ k}\Omega$ and $C = 2 \text{ nF}$, which have a corner frequency of about 80 kHz. The filters were made of tin- and lead-free surface-mount devices and mounted onto the connection board inside the vacuum close to the trap. The entire trap assembly was tilted slightly with respect to the laser beam access windows to allow for laser cooling along all three principal axes of the traps (see below).

The ^{24}Mg oven consisted of a steel tube of diameter $800 \mu\text{m}$ located a distance 4 cm away from the trap which was filled with solid pieces of ^{24}Mg , crimped shut at both ends, and cut open along a $150 \mu\text{m}$ by $700 \mu\text{m}$ slit. When resistively heated, it produced a vapor of neutral atoms that were directed at the traps in the horizontal direction (see inset of Fig. 1b). To load the traps, the neutral atoms were then photoionized, as described in more detail below.

The assembled trap package is placed on a connection board (see Fig. 2), which in turn is mounted inside a copper tube that forms part of a rf resonator that supplies the rf potential. The traps, Mg ovens, and copper tube reside inside a quartz envelope with extrusions and flat windows for laser beams and imaging of the trapped ions. The vacuum system is completed by a 20 liters/s ion getter pump, a Ti-sublimation pump and an ionization pressure gauge. The system was pumped to $5 \times 10^{-5} \text{ Pa}$ and baked-out at $210 \text{ }^\circ\text{C}$ for 8 days. After cooling the system to room temperature and several applications of Ti-sublimation, a base pressure of about $3 \times 10^{-9} \text{ Pa}$ was reached.

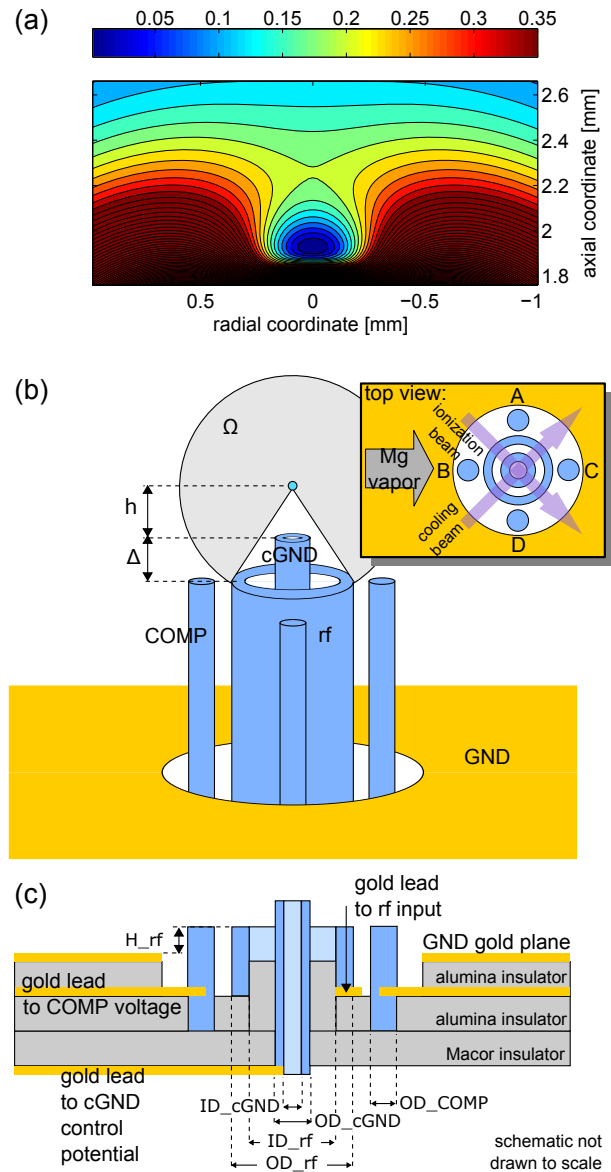


Figure 1: (a) Example calculation of the potential (in eV) for electrode configuration #3 using the corresponding parameters given in Table I and $^{24}\text{Mg}^+$ properties, while neglecting the compensation electrodes. Isoline separation is 25 meV and the axial coordinate is measured from the grounded plane (see figure part b). (b) Placement of the electrodes. The central ground electrode (cGND) is surrounded by the rf electrode and the grounded plane (GND). These electrodes provide the primary trapping potential. In addition four symmetrically placed compensation electrodes (COMP) provide fine adjustments to the overall potential. The distance h between the ion and the center electrode varies with the length difference Δ between the center electrode and the rf electrode. The accessible solid angle Ω is sketched as well [7]. The inset shows the position of the trap electrodes with respect to the laser beams for cooling and ionization. The direction from which the neutral Mg vapor enters the trapping region is indicated. (c) The layered assembly showing insulating planes with conducting gold leads and laser-cut holes to house the electrodes. Dimensions: $\text{OD_rf} = 710 \mu\text{m}$, $\text{ID_rf} = 535 \mu\text{m}$, $\text{OD_cGND} = 205 \mu\text{m}$, $\text{ID_cGND} = 100 \mu\text{m}$, $\text{OD_COMP} = 150 \mu\text{m}$, $H_rf = 1110 \mu\text{m}$.

IV. EXPERIMENTAL SETUP AND TRAP CHARACTERIZATION

Photoionization of neutral ^{24}Mg and Doppler cooling of the resulting $^{24}\text{Mg}^+$ ions was achieved by crossing three laser beams in the confinement region above the central electrode cylinder of a selected trap: The first laser beam at a wavelength of 285 nm (2 to 4 mW, 50 μm FWHM Gaussian waist size) was resonant with the $3s^2\ ^1S_0 \leftrightarrow 3s3p\ ^1P_1$ transition in neutral Mg. A second photon either at 285 nm or at 280 nm (below) promotes the electron from the $3s3p\ ^1P_1$ state to the continuum, producing a $^{24}\text{Mg}^+$ ion in the confinement region. For cooling, the second laser beam provided approximately 1 mW at 280 nm in a waist of approximately 30 μm . The laser frequency was tuned about 400 MHz below the $3s^2\ ^2S_{1/2} \leftrightarrow 3s3p\ ^2P_{1/2}$ transition of $^{24}\text{Mg}^+$ for initial cooling. A third, much weaker (2 to 10 μW) beam with intensity below saturation and tuned below the $3s^2\ ^2S_{1/2} \leftrightarrow 3s3p\ ^2P_{1/2}$ transition by half of the natural linewidth ($\simeq 20$ MHz) subsequently cooled the ions to near the Doppler limit. At that point photon scattering was dominated by the more closely detuned beam, and the farther detuned beam has little effect on the ion. However, in the case of sudden ion heating, for example due to a collision with background gas, the 400 MHz detuned beam could efficiently recool the ion to a point where the near-resonant beam will take over.

The degeneracy of motional frequencies in the radial direction was lifted by applying potentials on the order of 0.1 to 1 V to the compensation electrodes $A-D$. This created a static quadrupole field around the position of the ion with major axes at angles of about 45° relative to the two cooling beams (see inset in Fig. 1b). In addition, the entire trap assembly was tilted by about 7.5° with respect to the plane defined by the laser beams. This

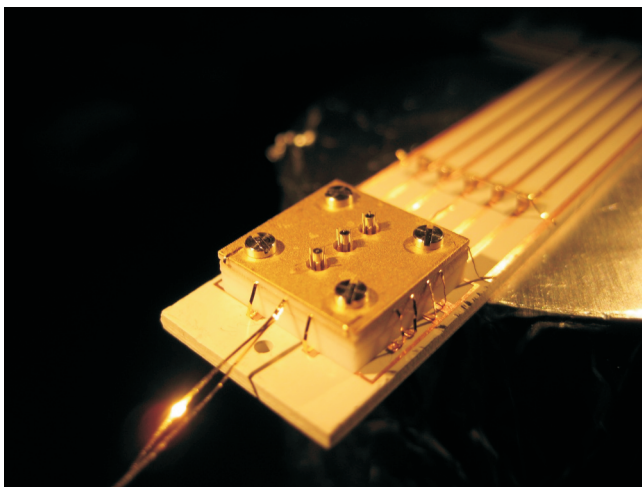


Figure 2: The completed trap assembly before insertion into the vacuum chamber. The three test traps with differing protrusion height Δ (increasing from front to back) of the central electrode can be seen.

Table I: Typical operating parameters for the three traps. The main difference between the three traps is the protrusion length Δ of the center electrode beyond the rf electrode. Due to this variation different trap frequencies and accessible solid angles are obtained. Some parameters (denoted by \blacktriangle) are difficult to measure directly and were inferred from the measured trap frequencies and the numerical simulation of the trapping potential.

electrode configuration	trap #1	trap #2	trap #3	unit
protrusion height Δ	0	250	500	μm
rf drive voltage U^{\blacktriangle}	290	460	400	V
rf drive frequency $\Omega_{\text{rf}}/(2\pi)$	80.15	31.94	11.85	MHz
trap frequencies:				
- axial	1.8	2.2	2.1	MHz
- radial \overline{AD}	0.951	1.268	1.064	MHz
- radial \overline{BC}	0.907	1.233	1.007	MHz
trap depth \blacktriangle	71	178	195	meV
ion to trap distance h	168	244	290	μm
accessible solid angle Ω [7]	71%	91%	96%	

ensured that the vertical axis of symmetry of the traps was not orthogonal to the wavevectors of the cooling laser beams. In this way all three normal modes of the ion were sufficiently cooled by a single laser beam.

Helical resonators [11] were driven by a low-noise signal generator to generate the rf trap potential. The helical resonators had loaded Q -factors ranging from 300 to 400 and were driven with input powers in the range of 16 to 32 dBm. With a voltage step-up factor of 20 (inferred from the resulting trap frequencies) this resulted in rf amplitudes in the range of 290 to 400 V.

The ion was imaged by detecting fluorescence from the cooling transition. The scattered photons were collected by a high numerical aperture ($\text{NA} \simeq 0.4$) objective located a distance of about 5 cm above the ion position in Fig. 1, and imaged onto an electron multiplying charge coupled device (EMCCD). Optionally, a photo-multiplier tube could be used for detection by redirecting the light from the objective with a switchable mirror.

In all three traps we observed ion lifetimes in excess of three hours under continuous laser cooling. Without cooling light, lifetimes were greater than 10 s.

The secular frequencies of ion motion along all three axes were determined by applying additional sinusoidal drive potentials to the compensation electrodes or the central electrode. If the drive frequency is in resonance with a secular frequency, ion motion is excited to large amplitudes, causing the level of laser induced fluorescence to drop sharply.

The operating parameters for each of the three traps are summarized in Table I together with the observed trap frequencies, the rf-drive voltage and the trap depth inferred from the trap frequencies and the numerical models for each trap.

To compensate micromotion due to electric stray fields, we varied the potential on all four compensation electrodes and the central tube while changing the power

level of the rf drive. Compensation was achieved when the ion position remained stationary for different rf drive amplitudes [6]. In addition, we could minimize micromotion along the direction of the cooling beam by maximizing the scattering signal close to resonance. By lowering the rf drive after loading we determined a minimum “stable” trapping rf power level which seemed to be limited only by background gas collisions. A trap loaded in configuration #3 was able to trap reliably after the trap well depth was lowered to less than 1 meV. For a well depth below room temperature ions can be lost by a single Langevin (charge-dipole) collision with a background gas atom. At the base pressure reached in our system, the mean ion lifetime with laser cooling on was around 30 s in this particular case.

V. LARGE SOLID ANGLE PHOTON ABSORPTION AND EMISSION

The trap geometry described in this paper permits optical access from a large solid angle. The compact design makes it possible to place the trap inside a metallic parabolic mirror that can also serve as an rf ground electrode (see Fig. 3a). In this way an ion may be placed at the focal point of the mirror and light emitted from the ion can be collected efficiently. Moreover, parallel light beams directed along the optical axis into the mirror can be focussed directly onto the ion. By appropriately shaping the transverse mode pattern of the incident light [12, 13] the field at the focus of the mirror can mimic a dipole excitation pattern, which could lead to a high coupling efficiency of photons to the ion [14].

Using electrode configuration #3 and a parabolic mirror with a depth to focal length ratio of 5.7:1 the solid angle from which scattered photons may be collected cov-

ers 65 % of the entire solid angle, more than could be achieved by an optical system based on a single imaging lens.

Since light emitted from a linear dipole transition does not propagate along the dipole axis, the same trap and mirror combination with the dipole axis along the mirror’s and trap’s vertical axis (see Fig. 1) would lead to a collection efficiency of 94 %. More importantly, light sent onto the ion in a dipolar pattern would be absorbed with the same high efficiency and thus provide a near perfect atom-to-photon coupling, possibly working down to the single-photon level [15].

VI. ION TRAP SURFACE SENSOR

The open upper half space of this trapping geometry suggests applications as a surface sensor. Surfaces of interest could be brought in proximity to the ion, as shown schematically in Fig. 3b. By either scanning the ion trap over the surface or translating the sample one could map out the electric and magnetic fields in proximity of the surface. The ion serves as a stylus probe tip that is extremely sensitive to electric fields oscillating at its motional frequencies. These frequencies can be tuned over at least two decades from approximately $\omega/(2\pi) = 100$ kHz to 10 MHz. In addition, information on the electric field direction can be extracted by utilizing all three nondegenerate modes of motion of the ion. At the same time, static and time-dependent magnetic fields can be measured by observing first and second order shifts of the ion on narrow internal transitions. While magnetic fields can be sensed closer to the surface and with higher signal-to-noise ratio with cold neutral atoms [16], a potential advantage of the ion sensor could be the combined sensitivity to electric and magnetic fields.

To estimate the sensitivity to AC electric fields we assume that the ion, initially cooled to its motional ground state, is coherently driven in resonance with a motional mode for the measurement time $t = 1/\Delta$, where Δ is the approximate measurement bandwidth. The amplitude α of the coherent state grows as [17]

$$\alpha = \frac{eEz_0}{2\hbar}t, \quad (1)$$

where E is the amplitude of the driving field, $z_0 = \sqrt{\hbar/(2m\omega)}$ is the size of the ion’s harmonic oscillator ground state wave function, e and m are the ion charge and mass, and \hbar is Planck’s constant. To yield a detectable signal this coherent excitation has to be comparable to the excitation due to motional heating that grows according to $\langle n_n \rangle = \langle \dot{n} \rangle t$ where $\langle \dot{n} \rangle$ is the ion’s heating rate [18]. This has typically been observed to be on the order of 1 quantum per millisecond for small room temperature traps (ion-electrode spacing of approximately 100 μm) with ion motional frequencies $\omega/(2\pi) = 1$ MHz. (For small cryogenic traps heating rates on the order of 1 quantum per second have been observed

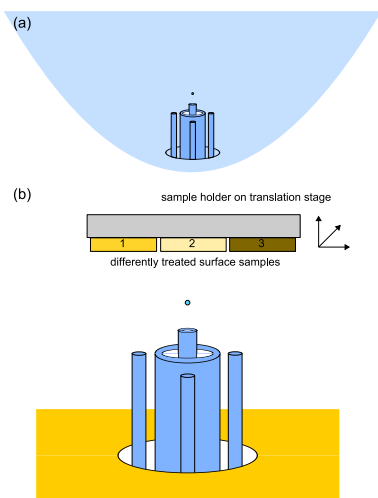


Figure 3: (a) Placement of the ion in the sharp focus of a parabolic mirror to maximize photon-ion coupling. (b) Scanning of different surfaces with the ion as a sensitive probe.

[19].) Assuming a signal-to-noise ratio of one, we require $\langle n_n \rangle = \langle n_c \rangle = |\alpha|^2$ and therefore

$$\frac{eE}{\sqrt{\Delta}} = \sqrt{\langle \dot{n} \rangle} \frac{2\hbar}{z_0}. \quad (2)$$

For $^{24}\text{Mg}^+$, $\langle \dot{n} \rangle = 1/\text{ms}$ and $\omega/(2\pi) = 1 \text{ MHz}$, this implies a force sensitivity of $0.46 \text{ yN}/\sqrt{\text{Hz}}$ ($0.46 \cdot 10^{-24} \text{ N}/\sqrt{\text{Hz}}$), several orders of magnitude below the smallest forces detectable with atomic force microscopes or micro-mechanical cantilevers [20]. This force sensitivity corresponds to an electric field sensitivity of $2.9 (\mu\text{V}/\text{m})/\sqrt{\text{Hz}}$. For a cryogenic ion trap where $\langle \dot{n} \rangle = 1/\text{s}$ the sensitivity would be increased by approximately 30.

To detect the local magnetic field at the position of the ion we may excite a narrow transition (for example a hyperfine transition) with well known field dependence. The method would have high spatial resolution, but be limited by the projection noise for measuring just a single two-level system [21]. On a Zeeman-shifted transition with a magnetic moment difference of 1 Bohr magneton, $\Delta\nu/\Delta B = 14 \text{ MHz}/\text{mT}$, when probed by the Ramsey method [22] with free precession time T_R , the magnetic field resolution ΔB is

$$\Delta B(\tau) = \frac{1}{2\pi(\Delta\nu/\Delta B)\sqrt{T_R\tau}} = 1.1 \times 10^{-11} T/\sqrt{\tau/s}, \quad (3)$$

where τ is the averaging time and the last expression assumes $T_R = 1 \text{ s}$. By actively compensating the surface field with external coils that lead to a known field geometry, we could detect not only the modulus but also the direction of the local magnetic field (vector magnetometer).

To estimate the spatial resolution of the ion probe we assume the surface to be probed is a conducting grounded plane. Modeling the ion trap in the presence of a ground plane located horizontally above the ion in Fig. 1 indicates that a stable quadrupole minimum is retained until

the distance to the surface is roughly equal to the distance of the ion to the center electrode. In the traps described in this paper, this would limit the ion to distances of about $170 \mu\text{m}$ from the surface, a limit that could be reduced by miniaturizing the trap. While the electric field in all space can be completely reconstructed from the field in one plane, this inversion is an ill-posed problem for spatial features much smaller than the ion-to-surface distance. Therefore the lateral spatial resolution when scanning the surface will be limited by the attained signal-to-noise ratio and is roughly equal to the distance to the surface if the signal-to-noise ratio is of order 1.

An application of the ion sensor that could be interesting for quantum information processing with trapped ions is to use it for straightforward comparisons of heating rates of different surfaces [18]. So far, to compare heating rates caused by different electrode surfaces, separate traps composed of different materials have been built and tested. This leads to uncertainties due to variations in the trap geometry, the exact steps of materials processing, surface contamination due to cleaning agents, and the bake-out procedure. Most of these variables could be eliminated, and the testing of different materials could be accelerated by use of one ion sensor on a variety of material samples deposited on the same carrier surface (see Fig. 3b).

Acknowledgments

This work was supported by IARPA and the NIST quantum information program. We thank C. Ospelkaus and S. Ospelkaus for comments on the manuscript. This paper is a contribution by the National Institute of Standards and Technology and not subject to U.S. copyright.

-
- [1] C. Schrama, E. Peik, W. Smith, and H. Walther, *Optics Communications* **101**, 32–36 (1993).
 - [2] L. Deslauriers, S. Olmschenk, D. Stick, W. K. Hensinger, J. Sterk, and C. Monroe, *Phys. Rev. Lett.* **97**, 103007 (2006).
 - [3] S. Stahl, F. Galve, J. Alonso, S. Djekic, W. Quint, T. Valenzuela, J. Verdu, M. Vogel, and G. Werth, *Europ. Phys. J. D* **32**, 139 (2004).
 - [4] J. R. Castrejoan-Pita, H. Ohadia, D. R. C. aand D. F. A. Winters, D. M. Segal, and R. C. Thompson, *J. Mod. Opt.* **11**, 1581 (2007).
 - [5] C. E. Pearson, D. R. Leibbrandt, W. S. Bakr, W. J. Mal-lard, K. R. Brown, and I. L. Chuang, *Phys. Rev. A* **73**, 032307 (2006).
 - [6] D. J. Berkeland, J. D. Miller, J. C. Bergquist, W. M. Itano, and D. J. Wineland, *J. Appl. Phys.* **83**, 5025–5033 (1998).
 - [7] Accessible solid angle ignores the compensation electrodes and outer ground plane. This seems reasonable because in future implementations, these electrodes could be made smaller and/or recessed below the rf electrode. This has not been done in the work reported here to facilitate construction of the basic electrode structure.
 - [8] D. Stick, W. K. Hensinger, S. Olmschenk, M. J. Madsen, K. Schwab, and C. Monroe, *Nature Physics* **2**, 36 (2006).
 - [9] S. Seidelin, J. Chiaverini, R. Reichle, J. J. Bollinger, D. Leibfried, J. Britton, J. H. Wesenberg, R. B. Blakestad, R. J. Epstein, D. B. Hume, et al., *Phys. Rev. Lett.* **96**, 253003 (2006).
 - [10] J. Britton, D. Leibfried, J. Beall, R. B. Blakestad, J. J. Bollinger, J. Chiaverini, R. J. Epstein, J. D. Jost, D. Kielpinski, C. Langer, et al., arXiv:quant-ph/0605170v1 (2006).
 - [11] W. M. Macalpine and R. O. Schildknecht, *Proc. IRE* **47**,

- 2099 (1959).
- [12] S. Quabis, R. Dorn, M. Eberler, O. Glöckl, and G. Leuchs, *Optics Communications* **179**, 1 (2000).
- [13] N. Lindlein, R. Maiwald, H. Konermann, M. Sondermann, U. Peschel, and G. Leuchs, *Laser Physics* **17**, 927–934 (2007).
- [14] M. Sondermann, R. Maiwald, H. Konermann, N. Lindlein, U. Peschel, and G. Leuchs, *Appl. Phys. B* **89**, 489–492 (2007).
- [15] M. Stobińska, G. Alber, and G. Leuchs, arXiv:0808.1666v1 [quant-ph] (2008).
- [16] M. Vengalattore, J. M. Higbie, S. R. Leslie, J. Guzman, L. E. Sadler, and D. M. Stamper-Kurn, *Phys. Rev. Lett.* **98**, 200801 (2007).
- [17] P. Carruthers and M. M. Nieto, *Am. J. Phys.* **33**, 537 (1965).
- [18] Q. A. Turchette, D. Kielpinski, B. E. King, D. Leibfried, D. M. Meekhof, C. J. Myatt, M. A. Rowe, C. A. Sackett, C. S. Wood, W. M. Itano, et al., *Phys. Rev. A* **61**, 063418 (1999).
- [19] J. Labaziewicz, Y. Ge, P. Antohi, D. Leibbrandt, K. R. Brown, and I. L. Chuang, *Phys. Rev. Lett.* **100**, 013001 (2007).
- [20] H. J. Mamin and D. Rugar, *Appl. Phys. Lett.* **79**, 3358 (2001).
- [21] W. M. Itano, J. C. Bergquist, J. J. Bollinger, J. M. Gilligan, D. J. Heinzen, F. L. Moore, M. G. Raizen, and D. J. Wineland, *Phys. Rev. A* **47**, 3554 (1993).
- [22] N. Ramsey, *Molecular Beams* (Oxford University Press, London, 1956).